JACS
JOURNAL OF THE AMERICAN CHEMICAL SOCIETY

Article

pubs.acs.org/JACS

Mechanism of Oxygen Activation in a Flavin-Dependent Monooxygenase: A Nearly Barrierless Formation of C4a-Hydroperoxyflavin via Proton-Coupled Electron Transfer

Surawit Visitsatthawong,[§] Pirom Chenprakhon,[†] Pimchai Chaiyen,[‖] and Panida Surawatanawong*[,§]

[§]Department of Chemistry and Center of Excellence for Innovation in Chemistry, Faculty of Science, [†]Institute for Innovative Learning, and [‖]Department of Biochemistry and Center of Excellence in Protein Structure and Function, Faculty of Science, Mahidol University, Bangkok 10400, Thailand

Supporting Information

ABSTRACT: Understanding how flavin-dependent enzymes activate oxygen for their oxidation and oxygenation reactions is one of the most challenging issues in flavoenzymology. Density functional calculations and transient kinetics were performed to investigate the mechanism of oxygen activation in the oxygenase component (C_2) of *p*-hydroxyphenylacetate 3-hydroxylase (HPAH). We found that the protonation of dioxygen by His396 via a proton-coupled electron transfer mechanism is the key step in the formation of the triplet diradical complex of flavin semiquinone and •OOH. This complex undergoes intersystem crossing to form the open-shell singlet diradical complex before it forms the closed-shell singlet C4a-hydroperoxyflavin intermediate (C4aOOH). Notably, density functional calculations indicated that the formation of C4aOOH is nearly barrierless, possibly facilitated by the active site arrangement in which His396 positions the proximal oxygen of the •OOH in an optimum position to directly attack the C4a atom of the isoalloxazine ring. The nearly barrierless formation of C4aOOH agrees well with the experimental results; based on transient kinetics and Eyring plot analyses, the enthalpy of activation for the formation of C4aOOH is only 1.4 kcal/mol and the formation of C4aOOH by C_2 is fast (~10^6 M^{-1} s^{-1} at 4 °C). The calculations identified Ser171 as the key residue that stabilizes C4aOOH by accepting a hydrogen bond from the H(N5) of the isoalloxazine ring. Both Ser171 and Trp112 facilitate H_2O_2 elimination by donating hydrogen bonds to the proximal oxygen of the OOH moiety during the proton transfer. According to our combined theoretical and experimental studies, the existence of a positively charged general acid at the position optimized for facilitating the proton-coupled electron transfer has emerged as an important catalytic feature for the oxygen activation process in flavin-dependent enzymes.

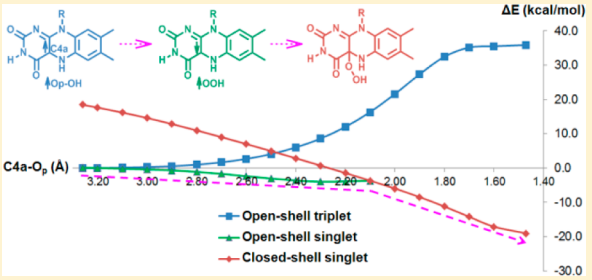

INTRODUCTION

Oxygen activation by enzymes has been a subject of great interest,[1] as it is a fundamental process involved in catabolic, anabolic, and xenobiotic processes in aerobic organisms[2] and has potential applications in both chemical and biochemical catalysis.[3] Cells employ key catalytic cofactors such as metals, pterins, and flavins to make a triplet dioxygen readily accepts electrons, resulting in active enzyme intermediates that can perform specific oxygenation or oxidation reactions.[3a,b] Flavin-dependent enzymes that can use oxygen as a substrate[4] are widely present in various cell types and are responsible for key biological catalytic reactions which generate functional groups such as hydroxyl, carbonyl, ketone, and epoxide groups.[5]

The enzymes that use oxygen as an electron acceptor are classified as oxidases, while those that perform oxygenation are termed oxygenases.[6] The oxygen activation reaction by flavin-dependent oxidases and oxygenases occurs without the involvement of transition metals. Regio- and stereospecific oxygen insertions by these enzymes are useful for industrial biocatalysis applications in the production of active pharmaceutical ingredients and fine chemicals.[7] Therefore, understanding the reaction mechanisms of these enzymes and determining the structural features which facilitate their oxygen activation are of prime interest such that these reactions can be improved and optimized to be compatible with additional applications.[8]

Interestingly, the rate constants of reduced flavin reacting with oxygen vary considerably among different flavin-dependent oxidases and oxygenases.[1e,4] The rate constant of free reduced flavin reacting with O_2 in aqueous solution[9] (~250 M^{-1} s^{-1} at 30 °C) is significantly lower than the rate constant for the same reaction, in which the flavin is bound to a flavoenzyme (up to 10^4 fold higher). For most of oxygenases, the reaction of reduced flavin and oxygen results in the formation of C4a-(hydro)peroxyflavin with rate constants ranging from ~10^4–10^6 M^{-1} s^{-1} at 4 °C, e.g., *p*-hydroxybenzoate hydroxylase (2.6 × 10^5 M^{-1} s^{-1}),[10] phenol hydroxylase (8.8 × 10^4 M^{-1} s^{-1}),[11] 2-methyl-3-hydroxypyridine-5-carboxylic acid oxygenase (5.6 × 10^4 M^{-1} s^{-1}),[12]

Received: April 27, 2015
Published: July 4, 2015

DOI: 10.1021/jacs.5b04328
J. Am. Chem. Soc. 2015, 137, 9363–9374

Scheme 1. Conventional Mechanisms for O_2 Activation in (a) Flavoenzyme Monooxygenases and (b) Flavoenzyme Oxidases and (c) The Newly Proposed Mechanism: Proton-Coupled Electron Transfer (PCET) for O_2 Activation, Requiring a Protonated His near the C4a Position (found as His548 in P2O and His396 in C_2 of HPAH)

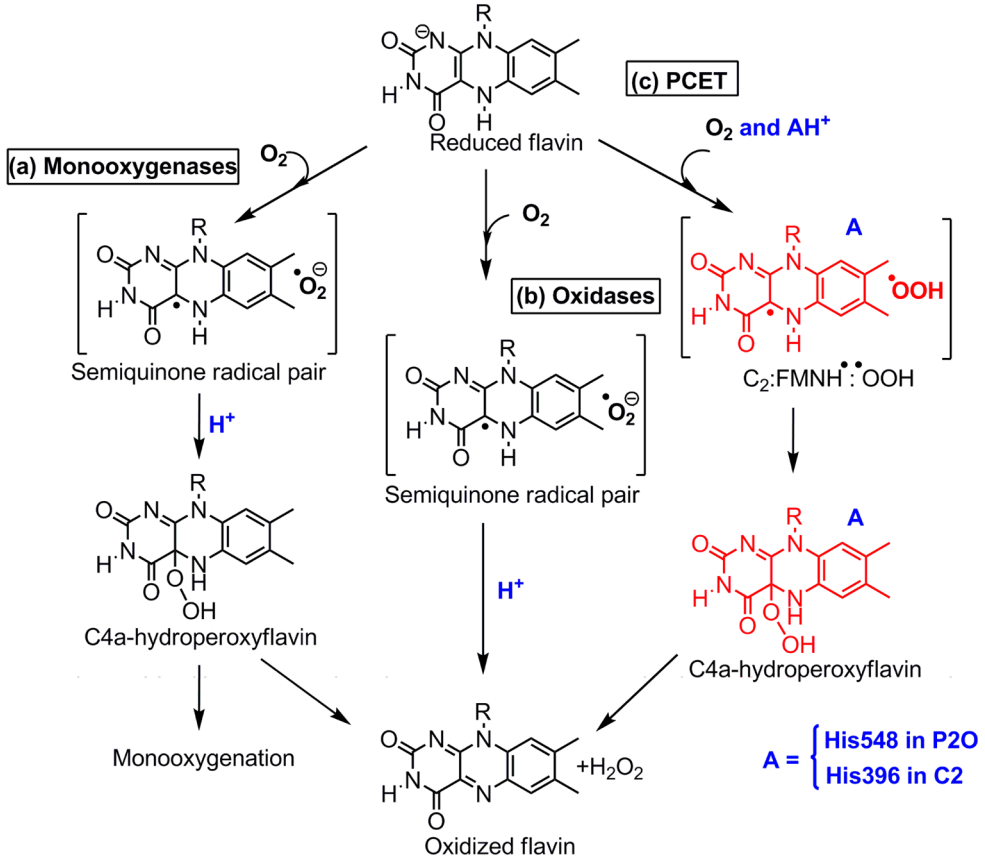

bacterial luciferase (1.95×10^6 M^{-1} s^{-1}),[13] cyclohexanone monooxygenase ($\geq 5 \times 10^6$ M^{-1} s^{-1}),[14] 3-hydroxybenzoate 6-hydroxylase (1.13×10^6 M^{-1} s^{-1}),[15] and the oxygenase component of *p*-hydroxyphenylacetate hydroxylase (C_2 of HPAH) (1.1×10^6 M^{-1} s^{-1}).[16]

In most oxidases, the reaction of reduced flavin and oxygen generally results in the direct formation of oxidized flavin and H_2O_2 (Scheme 1b).[4] The only exception was found in the reaction of pyranose 2-oxidase (P2O), in which C4a-hydroperoxyflavin (C4aOOH) was detected before the H_2O_2 elimination.[17] However, the rate constant of the reaction of reduced enzyme and oxygen by P2O is intermediate in magnitude (5.8×10^4 M^{-1} s^{-1})[17] as compared to those of the oxygenases previously mentioned. A key finding in the mechanism of oxygen activation by P2O has been recently reported: The conserved His548 acts as a general base in the first (reductive) half-reaction[18] and provides a proton in concert with an electron transfer for oxygen activation in the second (oxidative) half-reaction to form a diradical pair of flavin semiquinone and •OOH (Scheme 1c).[19] This is different from the conventional pathway for oxygen activation in flavin-dependent enzymes proposed by Bruice et al.[20] and Massey et al.,[4] where the protonation occurs after the C4a-peroxyflavin ($C4aOO^-$) stage (Scheme 1a,b).

The finding that proton-coupled electron transfer (PCET) is used as the means to activate oxygen in P2O has provided a new view on the oxygen activation mechanism in flavoenzymes and has raised many questions regarding this issue. It is currently unknown whether flavin-dependent monooxygenases, in which the rate constant of C4a-(hydro)peroxyflavin formation is generally large ($\sim 10^6$ M^{-1} s^{-1}), uses PCET as a mechanism to activate oxygen. Several studies have shown that a positively charged residue near the flavin C4a–N5 locus is one of the factors that facilitate oxygen activation in flavoenzymes.[21] The protonated His516 is important for increasing the oxygen reactivity in glucose oxidase.[22] For sarcosine oxidase, mutation of Lys265 to neutral methionine decreases the rate constant for the oxygen reaction by ~8000 fold,[23] while in fructosamine oxidase, similar mutation decreases the rate constant for the oxygen reaction by 550 fold.[24] Therefore, it is of interest to understand whether other enzymes that possess the conserved His or other proton-donor residues near the flavin C4a-position use the PCET mechanism at the first step of oxygen activation process as well.

p-Hydroxyphenylacetate hydroxylase (HPAH) is a two-component enzyme consisting of reductase (C_1) and oxygenase (C_2) components.[25] C_1 uses NADH to reduce FMN to generate $FMNH^-$. $FMNH^-$ is then transferred to C_2,[26] where the reaction with O_2 occurs. The C4aOOH is preferably formed before the binding of HPA; the bimolecular rate constant of C4aOOH formation in the absence of HPA (1.1×10^6 M^{-1} s^{-1}) is greater than in the presence of HPA (4.8×10^4 M^{-1} s^{-1}) (at pH 7 and 4 °C).[16] After the binding of HPA, C4aOOH incorporates a hydroxyl group into HPA to form 3,4-dihydroxyphenylacetate (DHPA).[27] In the absence of HPA, C4aOOH bound to C_2 is rather stable, with a rate constant for H_2O_2 elimination of 0.003 s^{-1}.[27a] A recent investigation has shown that His396, which is located near the C4a of the

DOI: 10.1021/jacs.5b04328
J. Am. Chem. Soc. 2015, 137, 9363−9374

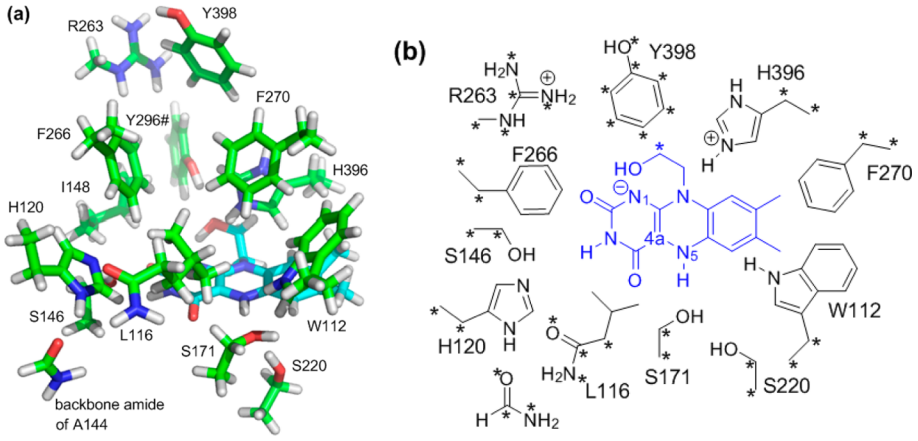

Figure 1. Active site model of C_2 in the "closed" conformation. Truncated $FMNH^-$ is in blue. (a) Three-dimensional structure of the active site model. (b) Schematic representation of the active site model. Constrained atoms are labeled with an asterisk. I148 and Y296# were omitted for clarity. All non-hydrogen atoms of I148 and Y296# were constrained. # indicates residues from subunit D.

isoalloxazine ring (the N^{ε} of His396 is ~4.6 Å from the flavin C4a position) is important for maintaining the high pK_a of the peroxide group of C4aOOH.[28] We speculated that this His residue could participate in a PCET mechanism similar to His548 in the reaction of P2O (the N^{ε} of His548 in P_2O is ~4.5 Å from the C4a).[29]

Therefore, in this work, the reaction of C_2 was used as a model to investigate the mechanism of oxygen activation in a flavin-dependent monooxygenase, in which the C4aOOH formation is rapid and robust. Density functional calculations, transient kinetics, and site-directed mutagenesis have shown that His396 in C_2 provides a proton for the PCET process. Notably, the formation of C4aOOH in C_2 is nearly barrierless. The finding that His396 in C_2 is in the optimum face-on position to interact with the O_2 molecule to generate and orient the $^{\bullet}$OOH radical toward the C4a of isoalloxazine ring reveals a new insight into the rapid formation of C4aOOH in a flavin-dependent oxygenase. Our findings suggest that in the presence of a positively charged general acid positioned at the proper site, PCET should be considered as a mechanism to facilitate O_2 activation.

EXPERIMENTAL PROCEDURES

Computational Details. All calculations were performed by density functional theory (DFT) using Gaussian09 program.[30] Gas-phase geometry optimizations were carried out with B3LYP[31]/6-31G(d).[32] Frequency calculations were performed for the transition states to ensure that there was one imaginary frequency corresponding to the reaction coordinate. Because some non-hydrogen atoms were constrained at the initial positions in the crystal structure during geometry optimization, all optimized structures are not strictly stationary points. Thus, zero-point vibrational energy corrections and thermal effects are not well-defined and were not considered in this study. B3LYP/6-311+G(d,p)[32] was used to calculate solvent corrections as single point energies with the conductor-like polarizable continuum model (CPCM)[33] and UAKS[34] radii (the dielectric constant of 4.0).[35] This calculation method has been successfully used in previous studies for the flavoenzyme mechanisms.[19,36] To compare with B3LYP/6-311+G(d,p), empirical dispersion correction[37] was included in the calculations of a single point energy and solvent correction by using B3LYP-D/6-311+G(d,p) for selected structures (Table S4).

Open-shell singlet and triplet states were treated with spin unrestricted DFT. Using a broken symmetry approach to treat the open-shell singlet states could lead to spin contamination from higher spin states. Therefore, we employed spin projection (SP)[38] to obtain the energy of the open-shell singlet species ($^{\text{singlet}}_{\text{SP}}E$) as shown in eq 1, where $^{\text{singlet}}E$ and $^{\text{triplet}}E$ are the electronic energies of the open-shell singlet and the triplet states, respectively. The coefficient C_{SC} is obtained from eq 2, where $^{\text{singlet}}\langle S^2\rangle$ and $^{\text{triplet}}\langle S^2\rangle$ are the expectation values for the total spin angular momentum of the open-shell singlet and the triplet states, respectively.

$$^{\text{singlet}}_{\text{SP}}E = {}^{\text{singlet}}E + C_{SC}[{}^{\text{singlet}}E - {}^{\text{triplet}}E] \quad (1)$$

$$C_{SC} = \frac{{}^{\text{singlet}}\langle S^2\rangle}{{}^{\text{triplet}}\langle S^2\rangle - {}^{\text{singlet}}\langle S^2\rangle} \quad (2)$$

The active site model is based on the X-ray crystal structure of the monooxygenase component (C_2) of HPAH with bound $FMNH^-$ in the absence of HPA substrate (2.80 Å; PDB code: 2JBS).[29a] This crystal structure is in a "closed conformation", in which Phe266, lying roughly perpendicular to Phe270, prevents substrate access to the active site in subunit A. Sucharitakul et al.[16] reported that the C4aOOH intermediate preferably formed before HPA binding. Therefore, a crystal structure without HPA was chosen to study the formation of the C4aOOH intermediate. The active site model taken from subunit A consists of an $FMNH^-$ (truncated at the C2′), the residues within ~8 Å radius from the C4a of isoalloxazine ring (His396, Trp112, Ser171, Leu116, Ser220, Phe270, Ile148, and Ser146), the residues that are important for HPA binding[29a] (Arg263, His120, Phe266, Tyr398, and Tyr296#) (# indicates the residue numbering in subunit D), and the backbone amide of Ala144, which provides hydrogen bonding to His120 (as residues around His can affect its pK_a)[39] (Figure 1).

The amino acid residues were truncated to include mainly their side chains and some of the backbone atoms. The established model consists of 234 atoms (Figure 1). Some non-hydrogen atoms were constrained at the initial positions of the crystal structure during geometry optimization of intermediates and transition states. As His396, Trp112, Leu116, Ser171, Ser220, and Phe270 are located above the isoalloxazine ring and are expected to be important in the reaction between O_2 and $FMNH^-$, these residues were constrained only at the α- and β-carbons to allow maximal side chain flexibility. Based on previous studies,[27c,40] Phe266 is important for controlling oxygen diffusion into the enzyme active site, and His120 and Ser146 are important for hydroxylation. Therefore, these residues were also constrained at the α- and β-carbons. To maximize computational time efficiency, Arg263, Tyr398, Ile148, Tyr296#, and the amide backbone of Ala144, all of which are more than 10 Å away from the flavin C4a-position, were constrained for all non-hydrogen atoms.

Regarding the protonation states of certain key residues, under the experimental condition of C_2 at pH 7,[16] Arg263 was chosen to be in the protonated form as Arg generally has pK_a of 12. Recently, Chenprakhon et al.[28] reported that His396 is important for

DOI: 10.1021/jacs.5b04328
J. Am. Chem. Soc. 2015, 137, 9363−9374

Scheme 2. Mechanism of O_2 Activation in the C_2 Active Site

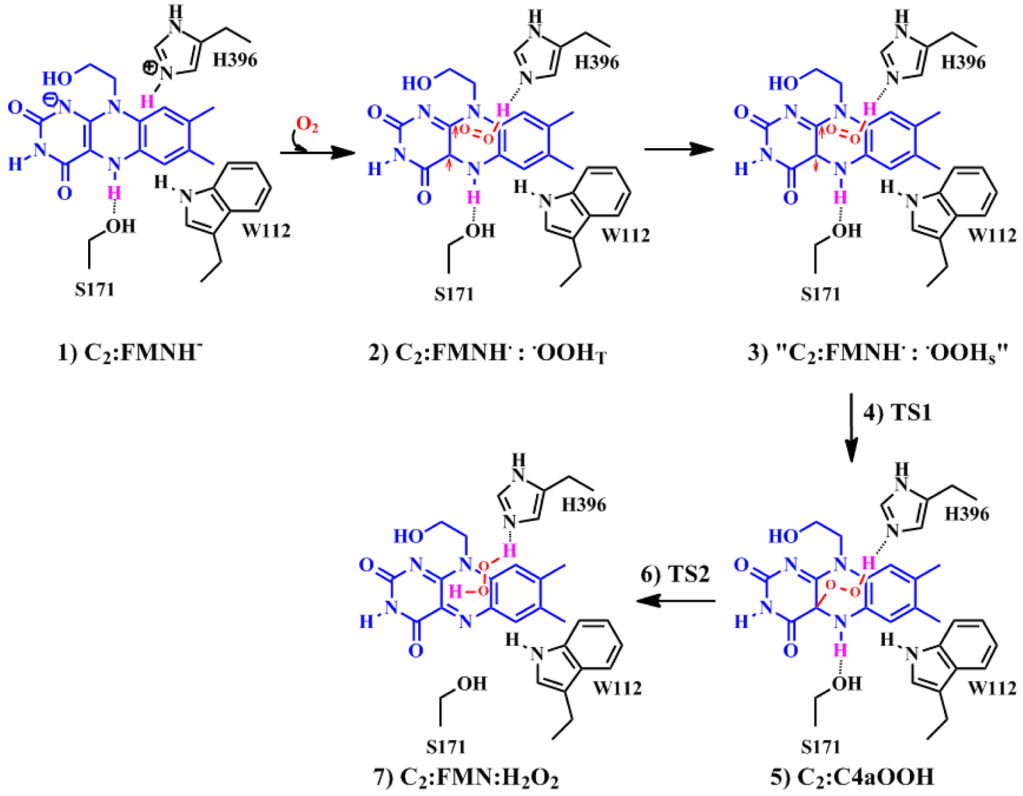

maintaining a protonated form and high pK_a of C4aOOH. Their study suggested that His396 may be a proton source for PCET and that initially His396 should be fully protonated before the oxygen reaction. Thus, His396 was assigned to be in a fully protonated form.

Temperature Dependence of C4a-Hydroperoxyflavin Formation and Decay in C_2. Rate constants of C4aOOH formation and decay in C_2 were measured according to the procedure previously described[16,27] using a stopped-flow spectrophotometer model SF-61DX2 (TgK Scientific, Bradford-on-Avon, U.K.) in single mixing mode. The optical path length of the observation cell was 1 cm. The stopped-flow instrument was made anaerobic by flushing the flow system with an oxygen scrubbing solution containing 10 mM sodium dithionite in 50 mM sodium phosphate buffer pH 7.0. The buffer was made anaerobic by equilibrating with oxygen-free nitrogen that has been passed through an oxyclear oxygen removal column (Labclear) in glass tonometers. The oxygen scrubbing solution was allowed to stand in the flow system overnight and was thoroughly rinsed with anaerobic buffer before the experiments were performed.

To study the effect of temperature on the reaction of C_2, the reactions were conducted at various temperatures (10−50 °C). A C_2 and FMN solution in 50 mM sodium phosphate buffer pH 7.0 was reduced by adding a solution of sodium dithionite while monitoring the FMN reduction using a UV−vis spectrophotometer inside the glovebox (Belle Technology). The resulting C_2:FMNH$^-$ complex was transferred into a glass tonometer and loaded onto the stopped-flow spectrophotometer. Air-saturated buffer at room temperature (oxygen concentration of 0.26 mM) was used as an oxygenated solution. The solution was placed in a syringe and loaded onto the stopped-flow spectrometer. The temperature of flow and mixing units was adjusted to 10, 20, 25, 30, 40, and 50 °C, and the solution was incubated for 20 min before the reaction started. As the oxygenated solution was kept under the closed system all the time and the limit of oxygen solubility at any temperatures is higher than 0.26 mM,[41] the setup thus maintained constant oxygen concentration.

After mixing, the reaction consisted of C_2 (50 μM), FMNH$^-$ (16 μM), and O_2 (0.13 mM). The reaction was monitored by measuring the absorbance at 390 and 450 nm to detect the C4aOOH intermediate and oxidized FMN, respectively. Apparent rate constants (k_{obs}) were analyzed using Program A (developed by R. Chang, C.-J. Chiu, J. Dinverno, and D. P. Ballou, at University of Michigan, Ann Arbor, MI). The enthalpy of activation ($\Delta H^{\ddagger}$) of the C_2 reaction was determined using the Eyring equation (eq 3), where R is the gas constant (1.987 cal mol^{-1} K^{-1}), k_B is the Boltzmann constant (1.381×10^{-23} J K^{-1}), h is Planck's constant (6.626×10^{-34}J s), T is the temperature (in K), and $\Delta S^{\ddagger}$ is the entropy of activation.[42] The data were analyzed through a linear plot of the rearranged Eyring equation as shown in eq 4, in which the value of enthalpy of activation can be determined from the slope of the plot of $\ln(k/T)$ versus $1/T$.

$$k = \left(\frac{k_B T}{h}\right) \exp\left(\frac{\Delta S^{\ddagger}}{R}\right) \exp\left(\frac{-\Delta H^{\ddagger}}{RT}\right) \tag{3}$$

$$\ln \frac{k}{T} = -\frac{\Delta H^{\ddagger}}{R}\frac{1}{T} + \ln \frac{k_B}{h} + \frac{\Delta S^{\ddagger}}{R} \tag{4}$$

Site-Directed Mutagenesis and Transient Kinetics Studies of the Trp112 Mutant. Single mutation of the Trp112 residue to alanine was performed using the QuickChange II Site-Directed Mutagenesis Kit according to the manufacturer's protocol (Stratagene, La Jolla, CA). The pET-11a plasmid containing the C_2-hpah gene was used as the template for mutagenic PCR. PCR reactions were carried out using various PCR instruments (GeneAmp PCR system, Applied Biosystem, model 2004 and MyCycler, Thermal Cycle, BIO RAD). The protocol for PCR and the sequences of the primers used containing the appropriate codons for generating the Trp112 mutant are described in the Supporting Information (Table S5). Expression and purification of the Trp112Ala mutant was performed in a similar manner as for the wild-type C_2.[16,27a] The plasmid containing the Trp112 mutant was transformed into *E. coli* BL21 (DE3) using heat-shock. *E. coli* BL21 (DE3) cells containing the Trp112 mutant plasmid were grown in 3.6 L of Luria−Bertani broth medium (LB) containing 50 μg/mL of ampicillin at 37 °C. When the OD_{600} of the culture reached ∼1.0, the temperature was adjusted to 25 °C and IPTG (isopropyl β-D-1-thiogalactopyranoside) was added into the culture to

DOI: 10.1021/jacs.5b04328
J. Am. Chem. Soc. 2015, 137, 9363−9374

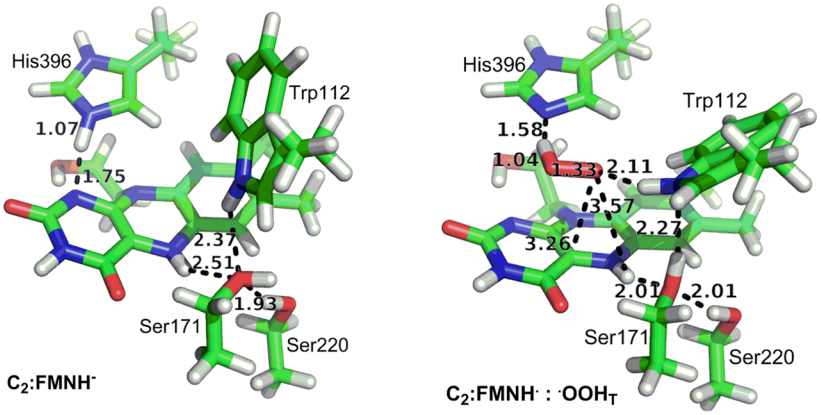

	C_2:FMNH$^-$ + free O_{2T}	C_2:FMNH$^{\bullet}$:$^{\bullet}$OOH$_T$
q_{flavin}	-0.740	-0.030
q_{O-O}	0.000[a]	-0.534
q_{OOH}	-	-0.050
q_{His}	+0.788[b]	+0.107[b]
ρ_{flavin}	0.000	+0.999
ρ_{OOH}	-	+1.003
d_{Op-Od} (Å)	1.21[a]	1.33
ΔE (kcal/mol)	0.0	-8.9

Figure 2. Optimized structures of C_2:FMNH$^-$ and C_2:FMNH$^{\bullet}$:$^{\bullet}$OOH$_T$. Some residues were omitted for clarity. Bond distances are shown in Å. The subscript T stands for the triplet state. Mulliken charge populations (q) on flavin (q_{flavin}), on His396 (q_{His}), on the two oxygen atoms of $^{\bullet}$OOH (q_{O-O}), and on $^{\bullet}$OOH(q_{OOH}) are shown. Mulliken spin populations (ρ) on flavin (ρ_{flavin}) and on $^{\bullet}$OOH (ρ_{OOH}) are shown. ΔE represents the solvent corrected relative energy with respect to C_2:FMNH$^-$ and free triplet oxygen (O_{2T}). [a]This value is from the free triplet oxygen (O_{2T}). [b]+0.788 and +0.107 correspond to the charge populations of fully and partially protonated His, respectively.

a final concentration of 1 mM to induce protein expression. The mutant enzyme was purified according to the protocol for wild-type C_2.[16,27a]

To study the reaction of the Trp112 variants with oxygen, the reactions were performed using a stopped-flow spectrophotometer model SF-61DX2 similar to the previous section. The reduced enzyme in 50 mM sodium phosphate buffer pH 7.0 was prepared inside the glovebox. The resulting W112A:FMNH$^-$ complex was transferred into a glass tonometer and loaded onto the stopped-flow spectrophotometer. The solution was mixed with buffers containing various concentrations of oxygen in the stopped-flow spectrophotometer. After mixing, the reaction contained W112A (40 μM), FMNH$^-$ (16 μM), and oxygen (0.13, 0.31, 0.61, 0.96 mM). The stopped-flow experiments were performed in single mixing mode at 4 °C. The stopped-flow reactions were monitored by measuring the absorbance changes at 390 and 450 nm to detect the formation and the decay of C4aOOH, respectively. Apparent rate constants (k_{obs}) were determined from the kinetic traces as described in the previous section.

RESULTS

Density Functional Study for the Reaction of the C_2:FMNH$^-$ Complex with Oxygen. To focus on the mechanistic feature of C_2 that is responsible for oxygen activation, the reaction of the C_2:FMNH$^-$ complex and oxygen in the absence of HPA was investigated. We found that this reaction consists of three steps: (i) O_2 activation, which involves a proton transfer from protonated His396 to the distal oxygen (O_d) in coupled with an electron transfer from FMNH$^-$ to form the triplet complex (C_2:FMNH$^{\bullet}$:$^{\bullet}$OOH$_T$); (ii) C4aOOH formation, where the C_2:FMNH$^{\bullet}$:$^{\bullet}$OOH$_T$ undergoes a spin transition to the open-shell singlet diradical before the bond between the C4a of the isoalloxazine ring and the proximal oxygen (O_p) of the $^{\bullet}$OOH moiety is formed to yield the C4aOOH intermediate; and (iii) H_2O_2 elimination, in which the proton at the N5 of isoalloxazine ring is transferred to the proximal oxygen of the OOH moiety to regenerate oxidized flavin (FMN) and H_2O_2 (Scheme 2).

O_2 Activation via PCET. The FMNH$^-$ in the C_2 active site model (C_2:FMNH$^-$) was calculated (Figure 2) based on the X-ray structure (PDB code: 2JBS),[29a] as described in the Computational Details. Fully protonated His396 was chosen because His396 was proposed to act as proton source for PCET process.[28] Mulliken charge populations on the flavin fragment, q_{flavin}, (−0.740) and on the fully protonated His396 fragment, q_{His}, (+0.788) are consistent with the expected negative charge on the reduced flavin (FMNH$^-$) and the positive charge on the fully protonated His396.

When the O_2 molecule is included in the cavity above the C4a position of C_2:FMNH$^-$ without orientational restraints, upon geometry optimization the proton from the fully protonated His396 is immediately transferred to the O_2, concomitant with the transfer of one electron from FMNH$^-$ to form a triplet C_2:FMNH$^{\bullet}$:$^{\bullet}$OOH$_T$ (Figure 2). In the C_2:FMNH$^{\bullet}$:$^{\bullet}$OOH$_T$, the H···N$^{\epsilon}$(His396) distance (1.58 Å) is extended from that of C_2:FMNH$^-$ (1.07 Å), while the O_d–H bond is formed (1.04 Å). Mulliken charge populations on the flavin fragment (q_{flavin}) change from rather negative (−0.740) in the C_2:FMNH$^-$ complex to almost neutral (−0.030) in the C_2:FMNH$^{\bullet}$:$^{\bullet}$OOH$_T$ (Figure 2), while those on the two oxygen atoms (q_{O-O}) change from neutral (0.000) in the free triplet oxygen (O_{2T}) to rather negative (−0.534) in the C_2:FMNH$^{\bullet}$:$^{\bullet}$OOH$_T$. In fact, the concomitant proton transfer neutralizes the negative charge on the two oxygen atoms of the

DOI: 10.1021/jacs.5b04328
J. Am. Chem. Soc. 2015, 137, 9363−9374

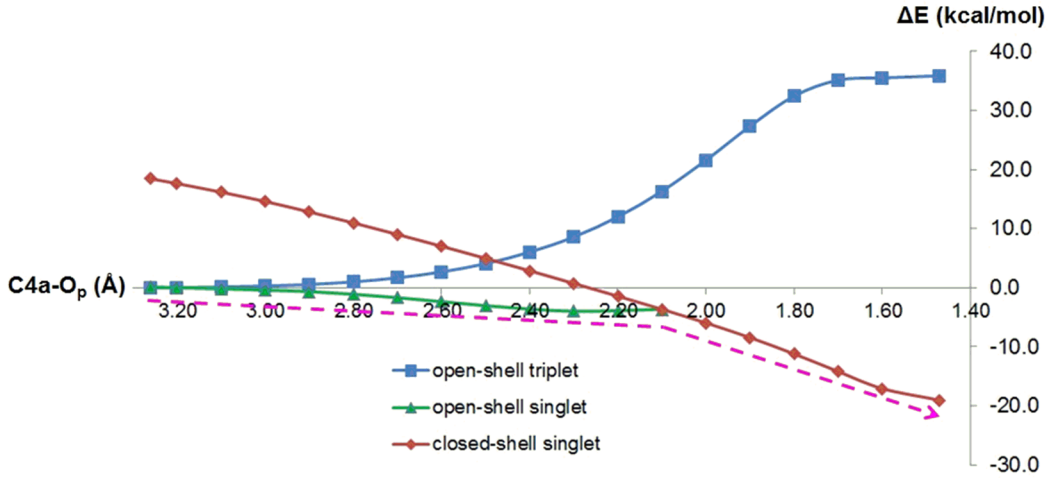

Figure 3. Relative gas-phase electronic energy (ΔE) profiles for the triplet (square), the open-shell singlet (triangle), and the closed-shell singlet (diamond) structures along the C4a−O_p bond formation path in C_2. The reaction path is proposed to be the pink dashed line. The gas-phase electronic energy for each structure is presented relative to that of C_2:FMNH$^\bullet$:$^\bullet$OOH$_T$ in kcal/mol.

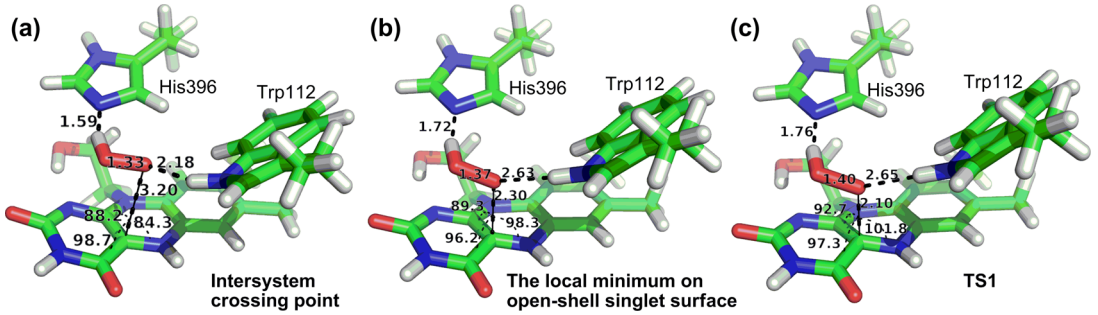

Figure 4. Calculated structures of the open-shell singlet species along the C4a−O_p bond formation path in C_2: (a) the structure at a C4a−O_p distance of 3.2 Å (approximate intersystem crossing point), (b) the structure at a C4a−O_p distance of 2.3 Å (approximate local minimum), and (c) the structure at a C4a−O_p distance of 2.1 Å (approximate transition state, TS1).

$^\bullet$OOH moiety, as the Mulliken charge population on the $^\bullet$OOH (q_{OOH}) is −0.050. The O−O bond is also elongated from 1.21 Å in the free triplet oxygen to 1.33 Å in C_2:FMNH$^\bullet$:$^\bullet$OOH$_T$. These results imply that an electron is transferred from the flavin to the $^\bullet$OOH fragment at this stage.

Mulliken spin populations on the $^\bullet$OOH (+1.003) and the flavin (+0.999) fragments (Figure 2) also support the electronic structure description for C_2:FMNH$^\bullet$:$^\bullet$OOH$_T$, in which it contains one unpaired electron on FMNH$^\bullet$ and one unpaired electron on $^\bullet$OOH with the same spin. Altogether, our data confirm that oxygen is activated by C_2:FMNH$^-$ via an electron transfer from the reduced flavin concomitant with a proton transfer from the protonated His396 to yield the triplet C_2:FMNH$^\bullet$:$^\bullet$OOH$_T$. Notably, His396 in C_2 plays a similar role as His548 in P2O[19] to provide a proton for the PCET process, which activates O_2 (Scheme 1c). The formation of C_2:FMNH$^\bullet$:$^\bullet$OOH$_T$ from C_2:FMNH$^-$ and dioxygen is favorable by −8.9 kcal/mol (Figure 2).

Formation of C4aOOH is a Nearly Barrierless Reaction. In the triplet C_2:FMNH$^\bullet$:$^\bullet$OOH$_T$, the C4a−O_p distance is 3.26 Å (Figure 2). The formation of the C4a−O_p bond would lead to the formation of a closed-shell singlet C4aOOH intermediate. This process is spin-forbidden.[4] To study the spin transition process, we tried to locate the stable structure of the open-shell singlet complex (C_2:FMNH$^\bullet$:$^\bullet$OOH$_S$), which corresponds to the triplet C_2:FMNH$^\bullet$:$^\bullet$OOH$_T$. However, all attempts simply led to the direct formation of the closed-shell singlet C4aOOH intermediate. Therefore, to search for the relevant intermediates and transition states for the formation of C4aOOH, we performed a relaxed potential energy surface scan on the C4a−O_p distance for the triplet, the open-shell singlet, and the closed-shell singlet states (Figure 3).

At the C4a−O_p distance of 3.26 Å, the energy of the open-shell singlet state is similar to that of the triplet C_2:FMNH$^\bullet$:$^\bullet$OOH$_T$ (+0.1 kcal/mol), while the closed-shell singlet state has a much higher energy (+18.5 kcal/mol) (Figure 3 and Table S3). Mulliken spin populations on the flavin and the $^\bullet$OOH of the open-shell singlet complex are −0.995 and +1.001, respectively (Table S1), suggesting that this species has a singlet diradical character, in which the flavin has one unpaired electron with a spin opposite to the other electron on the $^\bullet$OOH fragment. At the C4a−O_p distance of 3.20 Å, the energy of the triplet state is the same as that of the open-shell singlet state (Table S3). This could correspond to the approximate intersystem crossing point,[43] where the spin transition between the triplet and the open-shell singlet state can occur. The spin transition could be induced by the spin−orbit coupling as previously described for oxygen activation in the glucose oxidase model.[44]

As the C4a−O_p distance is shortened to form the C4aOOH intermediate, the energies for the triplet states increase, while the energies for the corresponding open-shell singlet states decrease (Figure 3). These energy changes suggest that the triplet C_2:FMNH$^\bullet$:$^\bullet$OOH$_T$ preferably undergoes a spin

DOI: 10.1021/jacs.5b04328
J. Am. Chem. Soc. 2015, 137, 9363−9374

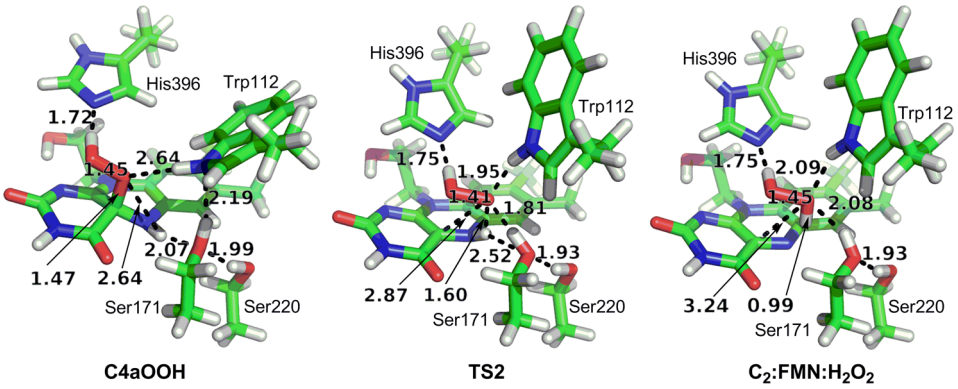

	C4aOOH	TS2	C_2:FMN:H_2O_2
q_{flavin}	+0.239	+0.408	+0.487
q_{O-O}	-0.800	-0.862	-0.973
q_{Op}	-0.320	-0.441	-0.498
d_{C4a-Op} (Å)	1.47	2.87	3.24
$d_{Op-H(N5)}$ (Å)	2.64	1.60	0.99
d_{C4a-N5} (Å)	1.41	1.33	1.30
d_{N5-H} (Å)	1.02	1.07	1.87
ΔE (kcal/mol)	-26.6	-9.4	-31.9

Figure 5. Optimized structures of C4aOOH, TS2, and C_2:FMN:H_2O_2. Some residues were omitted for clarity. Mulliken charge populations (q) on flavin (q_{flavin}), on two oxygen atoms of the OOH fragment (q_{OO}), and on O_p (q_{Op}) are shown. The C4a−O_p distance (d_{C4a-Op}), O_p−H(N5) distance ($d_{Op-H(N5)}$), C4a−N5 distance (d_{C4a-N5}), and N5−H distance (d_{N5-H}) are shown in Å. ΔE represents the solvent corrected relative energy of each species with respect to that of the C_2:FMNH$^-$ and the free triplet oxygen.

transition to the open-shell singlet state at the C4a−O_p distance of ∼3.2 Å, and then proceeds to form the C4a−O_p bond. As the C4a−O_p distance is shortened from 3.2 to 2.2 Å, the magnitude of the Mulliken spin populations on the flavin (q_{flavin}) and on the $^{\bullet}$OOH (q_{OOH}) gradually decrease from about −1.00 and +1.00 to −0.46 and +0.46, respectively, (Table S1). The diradical character of the open-shell singlet state diminishes as the C4a−O_p distance decreases. We could not locate the open-shell singlet diradical state at C4a−O_p distances <2.2 Å, as all of the structures converged to the closed-shell singlet state.

A rather flat energy surface was found for the open-shell singlet state with a shallow minimum at a C4a−O_p distance of 2.3 Å (Figure 3 and Table S3). This structure was approximated as a local minimum (Figure 4b).[45] Using the lowest energy path on Figure 3 as the reaction coordinate, the closed-shell singlet structure with a C4a−O_p distance of 2.1 Å could be approximated as a transition state (TS1) for the formation of C4aOOH (Figure 4c). Overall, the energy "barrier" for the formation of the C4aOOH is only +0.3 kcal/mol. Thus, the reaction is effectively barrierless. Finally, the C4a−O_p bond is completely formed; at the C4a−O_p distance of 1.47 Å, the closed-shell singlet C4aOOH intermediate is located. These results suggest that the open-shell singlet diradical structure "C_2:FMNH$^{\bullet}$:$^{\bullet}$OOH$_S$", once formed, is unstable and readily transforms to the closed-shell singlet C4aOOH intermediate. The formation of C4aOOH releases the energy of −26.6 kcal/mol, compared to C_2:FMNH$^-$ and the free triplet oxygen (Figure 5).

The C4aOOH intermediate has a longer O−O bond than that of C_2:FMNH$^{\bullet}$:$^{\bullet}$OOH$_T$ (1.45 Å versus 1.33 Å) (Figures 2 and 5), reflecting an increase in single bond character. Mulliken charge analysis indicates that the q_{flavin} changes from −0.030 to +0.239 and the q_{O-O} changes from −0.534 to −0.800 (Figures 2 and 5), implying that there is more electron delocalization from the flavin to the OOH fragment upon formation of the C4aOOH.

H_2O_2 Elimination. C4aOOH has three hydrogen-bond interactions from amino acid residues: (i) N$^{\varepsilon}$ of His396 accepts a hydrogen bond from the OOH moiety (1.72 Å); (ii) O$^{\gamma}$ of Ser171 accepts a hydrogen bond from the H(N5) of the isoalloxazine (2.07 Å); and (iii) N$^{\varepsilon}$H of Trp112 donates a hydrogen bond to the O_p of the OOH moiety (2.64 Å) (Figure 5). When the C4aOOH intermediate undergoes H_2O_2 elimination via transition state TS2, the C4a−O_p bond is cleaved as the C4a−O_p distance in TS2 is lengthened from that in C4aOOH (1.47 Å to 2.87 Å), while the O_p−H bond is formed as the O_p−H(N5) distance is shortened (2.64 Å to 1.60 Å). The C4a−N5 bond distances are also shortened (1.41 to 1.33 Å) as the sp^3 carbon becomes sp^2. The Mulliken charge population on the O_p (q_{Op}) becomes more negative in TS2 (−0.320 to −0.441) (Figure 5) to facilitate the proton abstraction at N5. The energy barrier for the H_2O_2 elimination relative to C4aOOH is +17.2 kcal/mol (Figure 5).

We have also performed B3LYP-D/6-311+G(d,p), which includes dispersion correction,[37] to compare with B3LYP/6-311+G(d,p) (Table S4). As calculated by B3LYP-D, C4aOOH becomes more stabilized (−4.5 kcal/mol), while TS2 is slightly destabilized (<1 kcal/mol). As a result, the B3LYP-D energy barrier (22.5 kcal/mol) is higher than the B3LYP energy barrier (17.2 kcal/mol) for the H_2O_2 elimination. Since the energy barrier from the transient kinetics experiment is 20.7 kcal/mol (*vide infra*), both B3LYP and B3LYP-D should be valid to describe this system.

Once the proton on N5 of isoalloxazine ring (H(N5)) is completely transferred to the OOH moiety to yield a complex of H_2O_2 and the oxidized flavin in C_2 (C_2:FMN:H_2O_2), the N5−H distance is lengthened to 1.87 Å and the O_p−H(N5) distance is shortened to 0.99 Å. Overall, the formation of C_2:FMN:H_2O_2 is favored by −31.9 kcal/mol. It is noteworthy

DOI: 10.1021/jacs.5b04328
J. Am. Chem. Soc. 2015, 137, 9363−9374

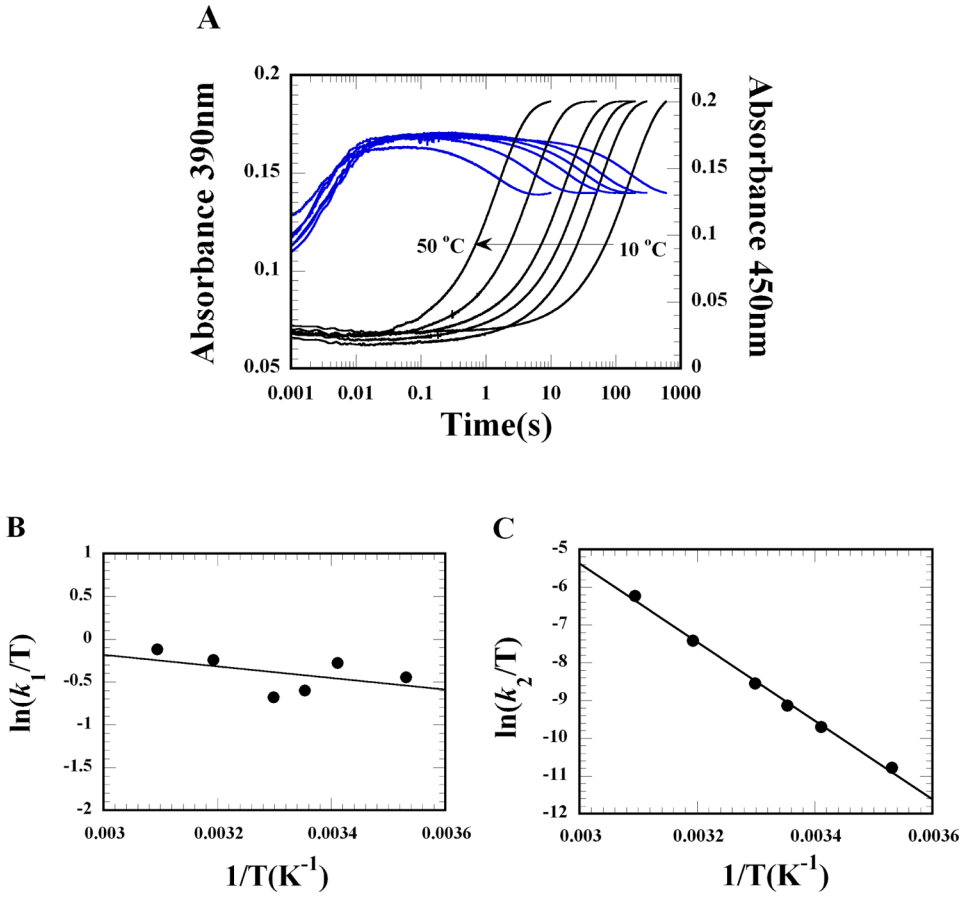

Figure 6. (A) Transient kinetics of the reaction of C_2:$FMNH^-$ with oxygen at various temperatures (10, 20, 25, 30, 40, and 50 °C). The absorbance at 390 nm is in blue, and the absorbance at 450 nm is in black. (B) Eyring plot of the rate constants for the C4aOOH formation; the enthalpy of activation ($\Delta H^{\ddagger}$) (+1.4 kcal/mol) is obtained from the slope according to eq 4. (C) Eyring plot of the rate constants for the H_2O_2 elimination; the enthalpy of activation ($\Delta H^{\ddagger}$) (+20.7 kcal/mol) is obtained from the slope according to eq 4.

that during the process of forming TS2, the hydrogen bond between the H(N5) and the O^{γ} of Ser171 is weakened (2.07 to 2.52 Å) and H(O^{γ}) of Ser171 forms a hydrogen bond with O_p of the OOH moiety (1.81 Å). For Trp112, the hydrogen bond between the $N^{\epsilon}H$ of Trp112 and the O_p of the OOH moiety is relatively strengthened (2.64 to 1.95 Å) (Figure 5). In this work, the site-directed mutagenesis of Trp112 has been performed to gain insights into its role as discussed below.

Activation Energy for the Reaction of C_2:$FMNH^-$ with O_2 Obtained by Eyring Plot Analysis. Transient kinetics for the reactions of C_2:$FMNH^-$ with oxygen at various temperatures (10−50 °C) was investigated using stopped-flow spectrophotometry to determine the enthalpy of activation ($\Delta H^{\ddagger}$) for the formation and the decay of C4aOOH. The reaction traces in Figure 6A show two phases. The first phase (0.001−0.01 s) is the formation of C4aOOH, reflected by an absorbance increase at 390 nm (blue trace). The second phase (0.1−600 s) is the elimination of H_2O_2 to form oxidized FMN, which is reflected by a decrease in the absorbance at 390 nm and an increase in absorbance at 450 nm (black trace). Rate constants of the H_2O_2 elimination step are clearly dependent on temperature. The higher the temperature, the greater the obtained rate constant value (Figure 6C). On the contrary, the rate constants of C4aOOH formation showed minimal temperature dependence (Figure 6B).

From the Eyring plots, the enthalpy of activation ($\Delta H^{\ddagger}$) of the C4aOOH formation was determined as +1.4 kcal/mol (Figure 6B), while the $\Delta H^{\ddagger}$ of the H_2O_2 elimination was determined as +20.7 kcal/mol (Figure 6C). Although the calculated electronic energy barriers for the formation of C4aOOH (+0.3 kcal/mol) and the elimination of H_2O_2 (+17.2 kcal/mol) (Figure 3 and Figure 5) were slightly underestimated as similarly published in other works,[46] the calculated energy barriers display the same trend for both reaction steps, in agreement with the experimental values. Altogether, the experimental data and the DFT calculations support that the formation of C4aOOH in C_2 is nearly barrierless.

Transient Kinetics for the Reaction of a Trp112 Variant of C_2 with Oxygen. In this study, the role of Trp112 in the formation and the stabilization of C4aOOH was investigated. Trp112 was replaced by alanine, and transient kinetics of this reduced enzyme (W112A:$FMNH^-$) with oxygen was performed at 4 °C using stopped-flow spectrophotometry to determine the rate of the C4aOOH formation and decay. The reactions were monitored at 390 and 450 nm. The reaction traces showed two phases (Figure 7A).

The first phase (0.001−0.04 s) of the reaction shows an increase in the absorbance at 390 nm (blue trace) with no change at 450 nm (black trace), and the observed rate constant is dependent on oxygen concentration. This phase represents the formation of C4aOOH. A plot of the observed rate constants (k_{obs}) of this phase versus oxygen concentrations is linear, consistent with a bimolecular rate constant of 6.4×10^5 M^{-1} s^{-1} (Figure 7B). This number is about 2-fold less than that

DOI: 10.1021/jacs.5b04328
J. Am. Chem. Soc. 2015, 137, 9363−9374

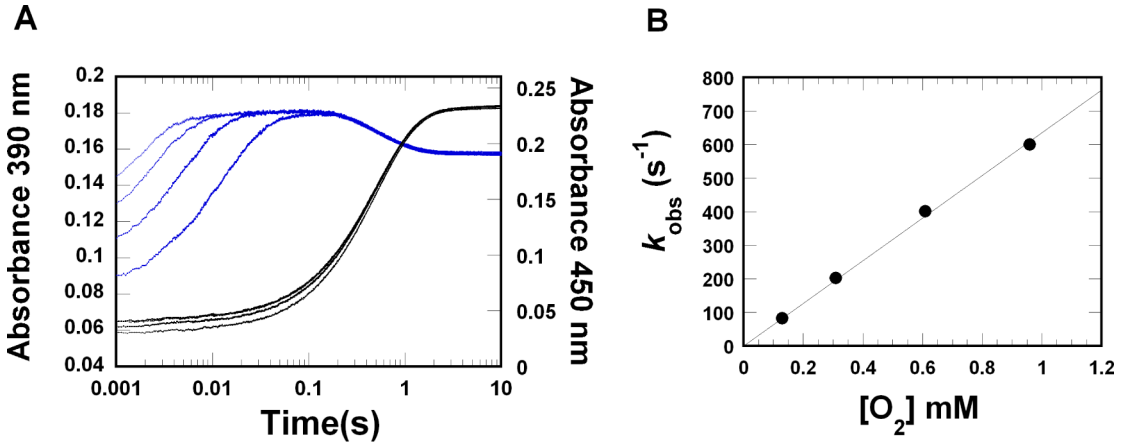

Figure 7. (A) Kinetic traces of the reaction of Trp112Ala:$FMNH^-$ with various concentrations of oxygen (0.13, 0.31, 0.61, and 0.96 mM) at 4 °C. The absorbance at 390 nm is in blue, and the absorbance at 450 nm is in black. (B) Plot of observed rate constant versus oxygen concentration. Bimolecular rate constant of C4aOOH formation was determined from a slope of the plot as 6.4×10^5 M^{-1} s^{-1}.

of the wild-type enzyme (1.1×10^6 M^{-1} s^{-1}). The second phase (0.04−10 s) shows a large increase in the absorbance at 450 nm and is independent of oxygen concentration. This phase is the H_2O_2 elimination step and is consistent with a rate constant of 1.9 s^{-1}. The rate is about 633-fold faster than that of the wild-type enzyme (0.003 s^{-1}). These results agree well with the DFT calculation in that Trp112 plays a minor role in the formation of C4aOOH but is important for the stabilization of C4aOOH.

DISCUSSION

Our DFT calculations give insights into the mechanism of oxygen activation by flavin-dependent monooxygenases. The prototype enzyme for this study, C_2, has a catalytic feature which facilitates a PCET mechanism for oxygen activation. The active site not only provides the protonated His396 for the PCET process but also supports the favorable formation of a flavin adduct through an almost barrierless transition state. All of theoretical studies were well verified by experimental data. Our findings explain how the flavin-dependent enzyme overcomes the barrier for activation of an oxygen molecule in order to result in fast and robust formation of C4aOOH.

PCET for dioxygen activation in C_2 is different from the path originally proposed by Massey and Bruice,[4,20b] which involves an electron transfer from the reduced flavin to dioxygen, resulting in a diradical pair of flavin semiquinone and superoxide anion that collapses to form the C4a−peroxide intermediate before undergoing a proton transfer to form C4aOOH (Scheme 1a). In contrast, the protonated His396 in C_2 is situated at the proper position to play the role as a general acid to provide a proton for PCET. The model proposed for the C_2 reaction is compatible with the absence of a solvent kinetic isotope effect (SKIE) for the formation of C4aOOH by this enzyme.[28] This implies that the proton transfer from His396 occurs rapidly before the formation of C4aOOH in C_2 and is not a rate-limiting step for the overall process of C4aOOH formation. The rate constants for the formation of C4aOOH formation in the H396N, H396A, and H396V variants were approximately 30-, 100-, and 300-fold slower than that of the wild-type enzyme, also agreeing with the catalytic role proposed for His396.[27b]

The PCET mechanism for the formation of C4aOOH was also reported for the reaction of pyranose 2-oxidase (P2O),[19] the only flavoenzyme oxidase in which the C4aOOH intermediate can be observed.[17] Interestingly, the active sites of P2O and C_2 share the similarity in the position of the protonated histidine above the C4a of the isoalloxazine ring: the N^{ε} of His548 in P2O and the N^{ε} of His396 in C_2 are located ∼4.5 and ∼4.6 Å from C4a, respectively.[29] Similar to Ser171 in C_2, Thr169 in P2O also has a hydrogen-bond interaction with H(N5) of the isoalloxazine ring to stabilize the C4aOOH intermediate. Despite the similarity in the presence of the His, oxygen activation in P2O is different from the reaction in C_2 in that the formation of C4aOOH in P2O needs to overcome a certain energy barrier (+6.3 kcal/mol),[19] while almost no barrier (+1.4 kcal/mol) exists for the formation of C4aOOH in C_2.

Why is the C4aOOH formation in the active site of C_2 very facile in comparison to P2O? During the C4aOOH formation process in P2O, the presence of His548 is required to provide a proton for the PCET. However, this alone is not sufficient for C4aOOH formation, as a hydrogen-bond interaction between the O_p and the $N^{\delta}H$ of Asn593 is also needed (Figure 8). Site-directed mutagenesis of either His548 or Asn593 leads to no observation of C4aOOH formation.[19] In C_2, His396, the corresponding residue to His548 of P2O, is a crucial residue for the formation of C4aOOH, while other residues such as Trp112, the corresponding residue to Asn593 of P2O, play only a minor role. The C4aOOH formation rate for wild-type C_2 is approximately 30-, 100-, and 300-fold higher than those of the H396N, H396A, and H396V variants, and only about 2-fold higher than that of the W112A variant as shown in this study.

The arrangement of the C4a−O_p distance and the angle of O_p−C4a−C10a to resulting in C4aOOH is probably a key factor responsible for the nearly barrierless reaction with oxygen in C_2. Unlike His548 in P2O, the position of His396 in C_2 is ideal for facilitating C4aOOH formation without requiring the participation from a neighboring residue, as is the case for P2O. In C_2, the hydrogen bonding between the $^{\bullet}$OOH and the N^{ε} of His396 positions the O_p directly above the C4a position of the isoalloxazine ring in a face-on[1e] configuration; the O_p−C4a−C10a angles are ∼90° for both the open-shell singlet complex at the C4a−O_p distance of 2.3 Å (approximate local minimum) and the closed-shell singlet complex at the C4a−O_p distance of 2.1 Å (approximate transition state, TS1) (Figure 4). Thus, the C4a−O_p bond can be formed effortlessly in C_2. On the other hand, despite of having two hydrogen bonds from

DOI: 10.1021/jacs.5b04328
J. Am. Chem. Soc. 2015, 137, 9363−9374

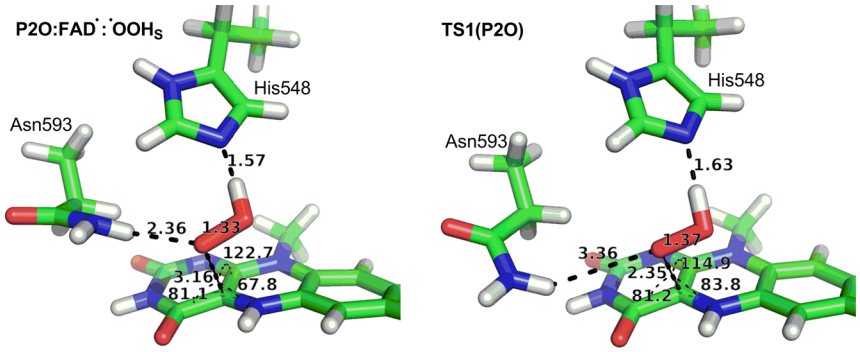

Figure 8. Optimized structures of the singlet diradical intermediate (P2O:FADH•:•OOH_S) and the transition state TS1(P2O) of P2O.

His548 and Asn593 interacting with the •OOH moiety at the *re*-face, the O_p of •OOH moiety in P2O is not directly above the C4a of the isoalloxazine of P2O:FADH•:•OOH_S (Figure 8), and the transition state for the C4a−O_p bond formation (TS1(P2O)) has the C4a−O_p bond tilted away from the plane perpendicular to the isoalloxazine ring; the O_p−C4a−C10a angle in TS1(P2O) is 115° (Figure 8). Correspondingly, an enthalpy of activation of 6.3 kcal/mol was found for the formation of C4aOOH in P2O by transient kinetics studies at various temperatures.[19]

After the proton transfer from the protonated His396 occurs concomitant with the electron transfer from $FMNH^-$, C4aOOH is readily formed, and the hydrogen bond between the N^{ε} of His396 and the O_d of •OOH fragment is retained (1.72 Å) (Figure 5). His396 not only donates a proton but also maintains the protonation state of C4aOOH so that it can act as an electrophile for HPA hydroxylation. The pK_a of C4aOOH in wild-type C_2 (9.8 ± 0.2) is higher than that of the H396V and H396A mutants (∼7).[28] Moreover, the rate constant for hydroxylation of HPA in wild-type C_2 was not significantly affected by pH, and ∼90% product yield was obtained throughout the pH range of 6.0−10.0.[27a]

Although His396 plays an important role in the formation of C4aOOH, it is not a significant contributor to the stability of C4aOOH. Previous site-directed mutagenesis investigations on C_2 showed that the rate for H_2O_2 elimination was not greatly affected in His396 variants.[27b] Correspondingly, in this work we found that both C4aOOH and TS2 are equally stabilized by His396; the hydrogen-bond interaction between the N^{ε} of His396 and the OOH fragment in C4aOOH and TS2 are similar (1.72 and 1.75 Å, respectively). During the H_2O_2 elimination process, apart from the C4a−O_p bond cleavage and O_p−H bond formation, the extent of hydrogen bond found in C4aOOH relative to the corresponding one in TS2 can affect the stability of C4aOOH. Generally, the stronger hydrogen bond on C4aOOH than the corresponding one on TS2 tends to favor C4aOOH stabilization, while the weaker hydrogen bond on C4aOOH than the corresponding one on TS2 tends to favor the elimination of H_2O_2 to form oxidized flavin.

The tight hydrogen bond between the O^{γ} of Ser171 and the H on the N5 of isoalloxazine in C4aOOH (2.07 Å) is weakened in TS2 (2.52 Å). This showed that Ser171 plays a key role in stabilizing C4aOOH via the hydrogen-bonding interaction between the H(N5) of the isoalloxazine ring and the O^{γ} of Ser171. Note that a hydrogen bond between H(O^{γ}) of Ser171 and O_p of the OOH moiety (1.81 Å) is formed in TS2 (Figure 5). This interaction facilitates H_2O_2 elimination, as it should stabilize OOH moiety after the C4a−O bond cleavage. Similarly, the tightened hydrogen bond between the O_p of the OOH moiety and H(N^{ε}) of Trp112 in TS2 (1.95 Å) (Figure 5) is also expected to assist H_2O_2 elimination. Therefore, H_2O_2 elimination in C_2 could be modulated by the interplay of the hydrogen-bond interaction with Ser171 and Trp112.

From the experiment, the rate constants for H_2O_2 elimination in S171A and S171T are approximately 1400- and 8-fold greater than that of the wild-type enzyme,[27b] and the rate constant for H_2O_2 elimination in W112A is approximately 633-fold greater than that of the wild-type enzyme. The alanine substitution of Ser171 or Trp112 may increase solvent accessibility to the flavin. From the study by Bach et al.,[47] the energy barrier for H_2O_2 elimination is rather high in the absence of local interactions, e.g., hydrogen bonds from amino acid residues. The energy barrier for H_2O_2 elimination can be reduced via a proton shuttle of water network. However, to identify the number and the position of water molecules involving in the process, the crystal structures of S171A and W112A variant enzymes are required.

The presence of a positively charged species has been thought to exert electrostatic stabilization of the anionic C4a−peroxyflavin intermediate in various flavin-dependent monooxygenases that require the nucleophilic flavin intermediate, e.g., Arg329 and $NADP^+$ in CHMO,[48] Arg342 and $NADP^+$ in steroid monooxygenase,[49] and Arg337 and $NADP^+$ in phenylacetone monooxygenase.[50] Here, we showed that the positively charged His396 of C_2 acts as a general acid for PCET to activate O_2. Another enzyme that catalyzes the same reaction as the C_2, the oxygenase component of 4-hydroxyphenylacetate 3-monooxygenase from *Thermus thermophilus* HB8 (HpaB),[51] has an Arg residue (Arg100) located ∼4.8 Å from C4a. The position of Arg100 in HpaB would allow it to act as a general acid similar to the role of His396 in C_2. This kind of systems could be of interest to investigate further whether they also use the PCET mechanism.

In summary, we give insights into the mechanism of O_2 activation in C_2 in the absence of HPA substrate (Scheme 2). C_2 has a protonated His in the active site and undergoes PCET for O_2 activation similar to P2O. However, the resulting diradical complex of flavin semiquinone and •OOH in P2O has to overcome a certain barrier to form C4aOOH, while the corresponding reaction in C_2 is nearly barrierless. We showed that the optimum position of His396 in C_2 places the O_p of the •OOH moiety in a position to directly attack the C4a of the isoalloxazine ring at a face-on configuration. These results correspond to the fact that the formation of C4aOOH in C_2 is more robust than in P2O. Once C4aOOH is formed, Ser171

DOI: 10.1021/jacs.5b04328
J. Am. Chem. Soc. 2015, 137, 9363−9374

plays a key role in both C4aOOH stabilization and H_2O_2 elimination, while Trp112 assists the elimination of H_2O_2. Overall, the calculated activation energies for the formation of C4aOOH and the elimination of H_2O_2 are in good agreement with the enthalpies of activation obtained from the Eyring plots. Our study suggests that for other flavoenzyme monooxygenases which have a positively charged general acid in the active site, the electrostatic positive charge may not be the only factor that facilitates O_2 activation, but the possibility of a PCET mechanism should also be considered.

■ ASSOCIATED CONTENT

Supporting Information

Summary of the relative electronic energies with solvation correction by B3LYP/6-31G(d), B3LYP/6-311+G(d,p), and B3LYP-D/6-311+G(d,p). The expectation values for the total spin angular momentum, $<S^2>$, and Mulliken spin populations on the flavin and on the OOH for the open-shell triplet and the open-shell singlet states of the C_2:FMNH$^{\bullet}$:$^{\bullet}$OOH with C4a-O distances of 3.26 Å to 1.47 Å. Nucleotide sequences used as primers for generating W112A mutants. Coordinates and calculated energies of all structures. The Supporting Information is available free of charge on the ACS Publications website at DOI: 10.1021/jacs.5b04328.

■ AUTHOR INFORMATION

Corresponding Author

*panida.sur@mahidol.ac.th

Notes

The authors declare no competing financial interest.

■ ACKNOWLEDGMENTS

Financial support from The Thailand Research Fund (TRF) (RTA5680001, TRG5780286 and TRG5780122), Development and Promotion of Science and Technology Talents Project (025/2555), Center of Excellence for Innovation in Chemistry (PERCH-CIC) and Faculty of Science, Mahidol University are gratefully acknowledged.

■ REFERENCES

(1) (a) Decker, A.; Solomon, E. I. *Curr. Opin. Chem. Biol.* **2005**, *9*, 152−163. (b) Bugg, T. D. H. *Curr. Opin. Chem. Biol.* **2001**, *5*, 550−555. (c) Mattevi, A. *Trends Biochem. Sci.* **2006**, *31*, 276−283. (d) Klinman, J. P. *Acc. Chem. Res.* **2007**, *40*, 325−333. (e) Chaiyen, P.; Fraaije, M. W.; Mattevi, A. *Trends Biochem. Sci.* **2012**, *37*, 373−380.

(2) (a) Dagley, S. *Annu. Rev. Microbiol.* **1987**, *41*, 1−23. (b) Zhao, Y.; Christensen, S. K.; Fankhauser, C.; Cashman, J. R.; Cohen, J. D.; Weigel, D.; Chory, J. *Science* **2001**, *291*, 306−309. (c) Laden, B. P.; Tang, Y.; Porter, T. D. *Arch. Biochem. Biophys.* **2000**, *374*, 381−388. (d) Poon, W. W.; Davis, D. E.; Ha, H. T.; Jonassen, T.; Rather, P. N.; Clarke, C. F. *J. Bacteriol.* **2000**, *182*, 5139−5146.

(3) (a) Teufel, R.; Miyanaga, A.; Michaudel, Q.; Stull, F.; Louie, G.; Noel, J. P.; Baran, P. S.; Palfey, B.; Moore, B. S. *Nature* **2013**, *503*, 552−556. (b) Liu, X.; Ryabenkova, Y.; Conte, M. *Phys. Chem. Chem. Phys.* **2015**, *17*, 715−731. (c) Armstrong, F. A.; Belsey, N. A.; Cracknell, J. A.; Goldet, G.; Parkin, A.; Reisner, E.; Vincent, K. A.; Wait, A. F. *Chem. Soc. Rev.* **2009**, *38*, 36−51.

(4) Massey, V. *J. Biol. Chem.* **1994**, *269*, 22459−22462.

(5) (a) Huijbers, M. M.; Montersino, S.; Westphal, A. H.; Tischler, D.; van Berkel, W. J. *Arch. Biochem. Biophys.* **2014**, *544*, 2−17. (b) van Berkel, W. J.; Kamerbeek, N. M.; Fraaije, M. W. *J. Biotechnol.* **2006**, *124*, 670−689.

(6) Fraaije, M. W.; Berkel, W. J. H. v. Flavin-Containing Oxidative Biocatalysts. In *Biocatalysis in the Pharmaceutical and Biotechnology Industries*, Patel, R. N., Ed.; CRC Press, Taylor & Francis Group: Boca Raton, FL, 2006; p 181.

(7) (a) Leisch, H.; Morley, K.; Lau, P. C. K. *Chem. Rev.* **2011**, *111*, 4165−4222. (b) Schmidt, S.; Scherkus, C.; Muschiol, J.; Menyes, U.; Winkler, T.; Hummel, W.; Gröger, H.; Liese, A.; Herz, H.-G.; Bornscheuer, U. T. *Angew. Chem., Int. Ed.* **2015**, *54*, 2784−2787. (c) Zhu, Y.; Zhang, Q.; Li, S.; Lin, Q.; Fu, P.; Zhang, G.; Zhang, H.; Shi, R.; Zhu, W.; Zhang, C. *J. Am. Chem. Soc.* **2013**, *135*, 18750−18753. (d) Hollmann, F.; Hofstetter, K.; Habicher, T.; Hauer, B.; Schmid, A. *J. Am. Chem. Soc.* **2005**, *127*, 6540−6541.

(8) (a) Zhang, Z.-G.; Lonsdale, R.; Sanchis, J.; Reetz, M. T. *J. Am. Chem. Soc.* **2014**, *136*, 17262−17272. (b) Brondani, P. B.; Dudek, H. M.; Martinoli, C.; Mattevi, A.; Fraaije, M. W. *J. Am. Chem. Soc.* **2014**, *136*, 16966−16969.

(9) Kemal, C.; Chan, T. W.; Bruice, T. C. *J. Am. Chem. Soc.* **1977**, *99*, 7272−7286.

(10) Entsch, B.; Ballou, D. P.; Massey, V. *J. Biol. Chem.* **1976**, *251*, 2550−2563.

(11) Maeda-Yorita, K.; Massey, V. *J. Biol. Chem.* **1993**, *268*, 4134−4144.

(12) Chaiyen, P.; Brissette, P.; Ballou, D. P.; Massey, V. *Biochemistry* **1997**, *36*, 8060−8070.

(13) Suadee, C.; Nijvipakul, S.; Svasti, J.; Entsch, B.; Ballou, D. P.; Chaiyen, P. *J. Biochem.* **2007**, *142*, 539−552.

(14) Sheng, D.; Ballou, D. P.; Massey, V. *Biochemistry* **2001**, *40*, 11156−11167.

(15) Sucharitakul, J.; Tongsook, C.; Pakotiprapha, D.; van Berkel, W. J. H.; Chaiyen, P. *J. Biol. Chem.* **2013**, *288*, 35210−35221.

(16) Sucharitakul, J.; Chaiyen, P.; Entsch, B.; Ballou, D. P. *J. Biol. Chem.* **2006**, *281*, 17044−17053.

(17) Sucharitakul, J.; Prongjit, M.; Haltrich, D.; Chaiyen, P. *Biochemistry* **2008**, *47*, 8485−8490.

(18) Wongnate, T.; Sucharitakul, J.; Chaiyen, P. *ChemBioChem* **2011**, *12*, 2577−2586.

(19) Wongnate, T.; Surawatanawong, P.; Visitsatthawong, S.; Sucharitakul, J.; Scrutton, N. S.; Chaiyen, P. *J. Am. Chem. Soc.* **2014**, *136*, 241−253.

(20) (a) Eberlein, G.; Bruice, T. C. *J. Am. Chem. Soc.* **1983**, *105*, 6685−6697. (b) Bruice, T. C. *Isr. J. Chem.* **1984**, *24*, 54−61.

(21) Gadda, G. *Biochemistry* **2012**, *51*, 2662−2669.

(22) Roth, J. P.; Klinman, J. P. *Proc. Natl. Acad. Sci. U. S. A.* **2003**, *100*, 62−67.

(23) Zhao, G.; Bruckner, R. C.; Jorns, M. S. *Biochemistry* **2008**, *47*, 9124−9135.

(24) McDonald, C. A.; Fagan, R. L.; Collard, F.; Monnier, V. M.; Palfey, B. A. *J. Am. Chem. Soc.* **2011**, *133*, 16809−16811.

(25) Chaiyen, P.; Suadee, C.; Wilairat, P. *Eur. J. Biochem.* **2001**, *268*, 5550−5561.

(26) Sucharitakul, J.; Phongsak, T.; Entsch, B.; Svasti, J.; Chaiyen, P.; Ballou, D. P. *Biochemistry* **2007**, *46*, 8611−8623.

(27) (a) Ruangchan, N.; Tongsook, C.; Sucharitakul, J.; Chaiyen, P. *J. Biol. Chem.* **2011**, *286*, 223−33. (b) Thotsaporn, K.; Chenprakhon, P.; Sucharitakul, J.; Mattevi, A.; Chaiyen, P. *J. Biol. Chem.* **2011**, *286*, 28170−28180. (c) Tongsook, C.; Sucharitakul, J.; Thotsaporn, K.; Chaiyen, P. *J. Biol. Chem.* **2011**, *286*, 44491−44502.

(28) Chenprakhon, P.; Trisrivirat, D.; Thotsaporn, K.; Sucharitakul, J.; Chaiyen, P. *Biochemistry* **2014**, *53*, 4084−4086.

(29) (a) Alfieri, A.; Fersini, F.; Ruangchan, N.; Prongjit, M.; Chaiyen, P.; Mattevi, A. *Proc. Natl. Acad. Sci. U. S. A.* **2007**, *104*, 1177−1182. (b) Kujawa, M.; Ebner, H.; Leitner, C.; Hallberg, B. M.; Prongjit, M.; Sucharitakul, J.; Ludwig, R.; Rudsander, U.; Peterbauer, C.; Chaiyen, P.; Haltrich, D.; Divne, C. *J. Biol. Chem.* **2006**, *281*, 35104−35115.

(30) Frisch, M. J.; Trucks, G. W.; Schlegel, H. B.; Scuseria, G. E.; Robb, M. A.; Cheeseman, J. R.; Scalmani, G.; Barone, V.; Mennucci, B.; Petersson, G. A.; Nakatsuji, H.; Caricato, M.; Li, X.; Hratchian, H. P.; Izmaylov, A. F.; Bloino, J.; Zheng, G.; Sonnenberg, J. L.; Hada, M.; Ehara, M.; Toyota, K.; Fukuda, R.; Hasegawa, J.; Ishida, M.; Nakajima, T.; Honda, Y.; Kitao, O.; Nakai, H.; Vreven, T.; Montgomery, J. A., Jr.; Peralta, J. E.; Ogliaro, F.; Bearpark, M. J.; Heyd, J.; Brothers, E. N.;

DOI: 10.1021/jacs.5b04328
J. Am. Chem. Soc. 2015, 137, 9363−9374

Kudin, K. N.; Staroverov, V. N.; Kobayashi, R.; Normand, J.; Raghavachari, K.; Rendell, A. P.; Burant, J. C.; Iyengar, S. S.; Tomasi, J.; Cossi, M.; Rega, N.; Millam, N. J.; Klene, M.; Knox, J. E.; Cross, J. B.; Bakken, V.; Adamo, C.; Jaramillo, J.; Gomperts, R.; Stratmann, R. E.; Yazyev, O.; Austin, A. J.; Cammi, R.; Pomelli, C.; Ochterski, J. W.; Martin, R. L.; Morokuma, K.; Zakrzewski, V. G.; Voth, G. A.; Salvador, P.; Dannenberg, J. J.; Dapprich, S.; Daniels, A. D.; Farkas, Ö.; Foresman, J. B.; Ortiz, J. V.; Cioslowski, J.; Fox, D. J. *Gaussian 09*, revision C.01; Gaussian, Inc.: Wallingford, CT, 2010.

(31) (a) Becke, A. D. *J. Chem. Phys.* **1993**, *98*, 5648−5652. (b) Lee, C.; Yang, W.; Parr, R. G. *Phys. Rev. B: Condens. Matter Mater. Phys.* **1988**, *37*, 785−789. (c) Stephens, P. J.; Devlin, F. J.; Chabalowski, C. F.; Frisch, M. J. *J. Phys. Chem.* **1994**, *98*, 11623−11627.

(32) (a) Hariharan, P. C.; Pople, J. A. *Theor. Chim. Acta* **1973**, *28*, 213. (b) Petersson, G. A.; Al-Laham, M. A. *J. Chem. Phys.* **1991**, *94*, 6081−6090. (c) Petersson, G. A.; Bennett, A.; Tensfeldt, T. G.; Al-Laham, M. A.; Shirley, W. A.; Mantzaris, J. *J. Chem. Phys.* **1988**, *89*, 2193−2218.

(33) Barone, V.; Cossi, M. *J. Phys. Chem. A* **1998**, *102*, 1995−2001.

(34) Barone, V.; Cossi, M.; Tomasi, J. *J. Chem. Phys.* **1997**, *107*, 3210−3221.

(35) Blomberg, M. R. A.; Siegbahn, P. E. M.; Babcock, G. T. *J. Am. Chem. Soc.* **1998**, *120*, 8812−8824.

(36) Wang, X. L.; Quan, J. M. *J. Am. Chem. Soc.* **2011**, *133*, 4079−4091.

(37) Grimme, S. *J. Comput. Chem.* **2006**, *27*, 1787−1799.

(38) Isobe, H.; Yamanaka, S.; Kuramitsu, S.; Yamaguchi, K. *J. Am. Chem. Soc.* **2008**, *130*, 132−149.

(39) (a) Harris, T. K.; Turner, G. J. *IUBMB Life* **2002**, *53*, 85−98. (b) Ranaghan, K. E.; Hung, J. E.; Bartlett, G. J.; Mooibroek, T. J.; Harvey, J. N.; Woolfson, D. N.; van der Donk, W. A.; Mulholland, A. J. *Chem. Sci.* **2014**, *5*, 2191−2199.

(40) Baron, R.; Riley, C.; Chenprakhon, P.; Thotsaporn, K.; Winter, R. T.; Alfieri, A.; Forneris, F.; van Berkel, W. J.; Chaiyen, P.; Fraaije, M. W.; Mattevi, A.; McCammon, J. A. *Proc. Natl. Acad. Sci. U. S. A.* **2009**, *106*, 10603−10608.

(41) Kolve, N. I. *Multiphase Flow Dynamics 4: turbulence, gas adsorption and release, diesel fuel properties*; Springer-Verlag: Berlin Heidelberg, 2011; p 210.

(42) Eyring, H. *J. Chem. Phys.* **1935**, *3*, 107−115.

(43) (a) Harvey, J. N.; Aschi, M.; Schwarz, H.; Koch, W. *Theor. Chem. Acc.* **1998**, *99*, 95−99. (b) Chachiyo, T.; Rodriguez, J. H. *J. Chem. Phys.* **2005**, *123*, 094711−094719.

(44) Prabhakar, R.; Siegbahn, P. E. M.; Minaev, B. F.; Agren, H. *J. Phys. Chem. B* **2002**, *106*, 3742−3750.

(45) Kraka, E.; Cremer, D. *Acc. Chem. Res.* **2010**, *43*, 591−601.

(46) Kubas, A.; De Sancho, D.; Best, R. B.; Blumberger, J. *Angew. Chem., Int. Ed.* **2014**, *53*, 4081−4084.

(47) Bach, R. D.; Mattevi, A. *J. Org. Chem.* **2013**, *78*, 8585−8593.

(48) Polyak, I.; Reetz, M. T.; Thiel, W. *J. Am. Chem. Soc.* **2012**, *134*, 2732−2741.

(49) Franceschini, S.; van Beek, H. L.; Pennetta, A.; Martinoli, C.; Fraaije, M. W.; Mattevi, A. *J. Biol. Chem.* **2012**, *287*, 22626−22634.

(50) Orru, R.; Dudek, H. M.; Martinoli, C.; Torres Pazmino, D. E.; Royant, A.; Weik, M.; Fraaije, M. W.; Mattevi, A. *J. Biol. Chem.* **2011**, *286*, 29284−29291.

(51) Kim, S. H.; Hisano, T.; Takeda, K.; Iwasaki, W.; Ebihara, A.; Miki, K. *J. Biol. Chem.* **2007**, *282*, 33107−33117.

DOI: 10.1021/jacs.5b04328
J. Am. Chem. Soc. 2015, 137, 9363−9374